Hindawi
International Journal of Photoenergy
Volume 2021, Article ID 5581081, 13 pages
https://doi.org/10.1155/2021/5581081

Research Article

Influence of Narrow Rectangular Channel (AR = 1 : 4) on Heat Transfer and Friction for V- and W-Shaped Ribs in Turbine Blade Applications

Karthik Krishnaswamy,[1] **Suresh Sivan**,[1] **and Hafiz Muhammad Ali**[2]

[1]*Mechanical Engineering, National Institute of Technology, Tiruchirappalli 620015, India*
[2]*Mechanical Engineering, King Fahd University of Petroleum and Minerals, Dhahran 31261, Saudi Arabia*

Correspondence should be addressed to Suresh Sivan; ssuresh@nitt.edu

Received 13 January 2021; Revised 8 May 2021; Accepted 17 May 2021; Published 25 May 2021

Academic Editor: Gianluca Coccia

Effective cooling of blades with a nominal pressure drop is essential for performance augmentation and thermal management of gas turbines. Hence, present work is aimed at determining the heat transfer enhancement and friction for W- and V-shaped ribs inside a rectangular cooling channel having hydraulic diameter (D_h) of 0.048 m and aspect ratio (AR) 1 : 4. Ribs are fixed facing downstream with angle of attack (α) 45° on opposite walls. Pitch (P) between two successive ribs is 25 mm for both cases. Continuous V- and W-shaped ribs with height to channel hydraulic diameter ratio (e/D_h) 0.052 and 0.0416 and pitch to height ratio (P/e) 10 and 12.5, respectively, have been examined for Reynolds number (Re) range 20000-80000. Heat transfer augmentation achieved at Re 80000 is 1.94 and 1.8 times higher than Re 20000 for V- and W-shaped ribs, respectively. Streamwise and spanwise variations in local Nusselt number ratio are highest for V-shaped ribs, which are estimated to be 31% and 12%. For W-shaped ribs, variations are 17.5% and 3.5%. Nusselt number (Nu) is highest along span length $0.5w$ for V-shaped ribs due to dominance of apex induced secondary flow. For W-shaped ribs, Nusselt number along the span lengths is found to be nearly same view uniformity in secondary flow. Maximum enhancement ($\mathrm{Nu/Nu}_o$) estimated for both the rib shapes is 3.9 at Re 20000. Due to increased rib height, friction losses for V-shaped ribs are higher than W-shaped ribs. Maximum friction loss increment is estimated to be 85% for V-shaped ribs and 42% for W-shaped ribs between Re 20000 and 40000. For both rib shapes, impact of ribs is found to be greatest at Re 40000. Thermohydraulic performance (THP) for W-shaped ribs is superior to V-shaped ribs. Best THP achieved for W- and V-shaped ribs are 3.7 and 3.4 at Re 20000.

1. Introduction

Gas turbine engines propel aircraft, ships, and automobiles. In addition, they are also extensively used for power generation. The efficiency and output of these engines are dependent upon the Turbine Inlet Temperature (TIT). Increase in TIT will result in increased power output. The present generation turbines are already operating closer to melting point, and therefore, any further increase in TIT is possible only through efficient thermal management. The cooling of inner and outer blade surfaces is done by withdrawing a small quantity of compressed air. Withdrawal of air impacts the output and efficiency. Hence, the aim of various cooling techniques is to attain more heat transfer with marginal drop in pressure, thereby reducing the coolant consumption. Rib cooling is one amongst the cooling techniques used for heat removal from midsection of turbine blade. For years, many researchers have examined the thermohydraulic performance generated due to ribs in turbine blade cooling channels which are generally rectangular, trapezoidal, and square in cross section. Studies have established that various geometrical parameters like channel cross section, rib height, coolant angle of attack, pitch between the ribs, rib profile, and number of walls with ribs influence the friction and heat

transfer. Results presented by few studies are discussed in succeeding paragraphs.

Goodarzi et al. [1] investigated convective heat transfer for flow inside cavity and stated that magnitude of heat transfer depends largely on effects of hydrodynamic and thermal boundary layers between the fluid and the surface. Also, majority of the studies impose constant heat flux condition on the surface to study the heat transfer phenomenon. Goodarzi et al. [2] stated that in comparison to experimental methods, computational methods are simpler, economical, and safe for understanding heat transfer and fluid flow problems. Abraham and Vedula [3] by using a converging channel examined friction and heat transfer with 45° W- and V-shaped ribs. Examination revealed that heat transfer coefficients varied more for V-shaped ribs because of cross stream flows, and performance of both rib shapes was within uncertainty limits for optimum P/e of 10. Prashant et al. [4] studied different ribs fixed in an aspect ratio 1 : 1 cooling channel for Re 19500 to 69000 and concluded that V-shaped and angled ribs at 45° to coolant flow provided greatest performance. Ghodake et al. [5] evaluated augmentations for different ribs using rectangular duct and confirmed that broken V-shaped and rectangular tape ribs with P/e of 8.3 generated higher augmentations. Heat transfer and pressure loss characteristics were investigated for AR 1 : 1 channel with high blockage ratio ribs by Yang et al. [6]. The ratio of P/e ranges from 5 to 15, and Re ranged from 1400 to 9000. Their analysis indicated that as Re increased, heat transfer coefficients and pressure losses increased. Furthermore, they concluded that symmetric arrangement ribs showed higher heat transfer and pressure losses than staggered arrangement ribs. For a revolving two pass square cross section cooling channel with staggered 45° ribs, friction and heat transfer behaviour were presented by Deng et al. [7]. The Re ranged from 20000 to 60000, and rotation number ranged 0 to 1.02. The results showed that 45° ribs with P/e ratio 10 enhanced heat transfer by 15-65% for smooth walls and 40-80% for ribbed walls. The pressure drop in ribbed channel was found 1.5-2.1 times higher than smooth channel. Further, the authors showed that when the rotation number exceeds 0.25, thermal performance considerably improved due to rotation effects. Prashant et al. [8, 9] compared the effects due to ribs on single wall and two walls of a square channel. For Re 20000, V-ribs fixed on two walls produced greater augmentation, and the trailing wall heat transfer in rotating condition was highest due to Coriolis effects. The influence on heat transfer due to 45° V-ribs in 1 : 2 aspect ratio channel for Re range 25000 to 75000 revealed that heat transfer increased in the flow direction view greater turbulent mixing, and the heat transfer was highest at the bend. Ravi et al. [10] numerically investigated four different rib profiles placed inside a square cross section channel at 45° to flow direction. The authors presented that 45° V-shaped and angled ribs exhibited best performance for the Re range 20000 to 70000.

For different aspect ratios and working conditions, impact of 45° ribs on heat transfer and flow was investigated numerically by Longfei et al. [11]. The aspect ratios of the ribbed channels studied were 1 : 2, 1 : 1, and 2 : 1, respectively. According to their findings, heat transfer area increases because of ribs, and hence, the heat transfer increases. Their evaluation revealed that heat transfer area due to ribs increased by 30%, and overall heat transfer improved by 50%. Also, the pressure loss in 1 : 2 AR channel with same hydraulic diameter as 2 : 1 AR channel was found to be 60% less. Prashant et al. [12] using an AR 1 : 1 channel studied the effect of criss-cross pattern rib turbulators positioned in an inline and staggered configurations. They concluded that heat transfer enhancement was nearly same for inline and staggered configurations; however, friction for inline configuration was lower than staggered configuration. For Re range 30000 to 60000, heat transfer enhancement ranged from 2.7 to 3.1, and thermal performance ranged from 1.2 to 1.5. Sebastian and Arbeiter [13] conducted an analysis of heat transfer and turbulent flow for V-shaped ribs with e/D_h of 0.0638 and transverse ribs with e/D_h of 0.0652 fixed on one wall. According to their findings, at Re 100000, upstream pointing V-shaped ribs produced best thermal performance and heat transfer enhancement. Effect of rib orientation on flow and thermal parameters was investigated by Liou et al. [14] inside a two pass parallelogram channel. The blockage ratio was 0.1, and P/e was 10. For Re range 5000 to 20000, thermal performance of 45° angled ribs was found to be best. Heat transfer and fluid flow due to different discrete ribs were investigated by Wang et al. [15] in a revolving rectangular channel with AR 2 : 1. The blockage ratio was 0.1, and P/e was 10. They concluded that presence of streamwise rib gap improved the heat transfer however, with increase in the gap increment in heat transfer declined. In addition, they established that the increase in spanwise rib gap reduced the pressure drop; however, heat transfer augmentation is restricted. Aghaei et al. [16] evaluated the impact of baffles on flow inside an enclosure and confirmed that entropy reduces the efficacy, and hence, it is important to establish the entropy for enhancing the efficiency of machines. Further, the authors brought out that researchers are working towards minimizing the entropy for achieving optimal performance. Patil and Borse [17] brought out that the heat transfer in turbine blade midsection is enhanced by fixing ribs inside the serpentine cooling passages. They also brought out in their review that narrow channel having AR 1 : 4 produced lower friction penalties than aspect ratios 1 : 2, 1 : 1, and 2 : 1 channels. Aboghrara et al. [18] reiterated the fact that heat transfer due to convection can be enhanced by incrementing the contact area and also by increasing the turbulent mixing by introducing roughness elements in the flow path. Omeroglu [19] evaluated the thermal enhancement inside a photovoltaic/thermal collector by using fin turbulators. The author established that with increase in Reynolds

Table 1: Details of rib geometry.

Ribs	e (mm)	P/e	e/D_h	α (°)	Recommended range in literature		
					P/e	e/D_h	α (°)
V	2.5	10	0.052	45°	5-15	0.05-0.1	30°-60°
W	2	12.5	0.0416	45°			

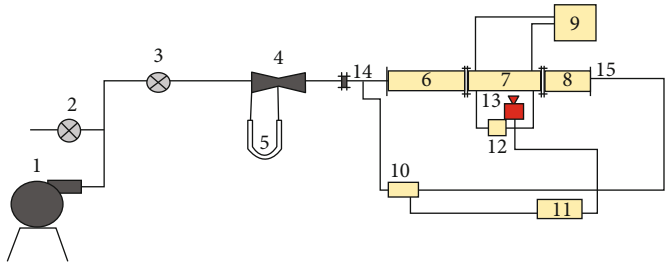

1. Centrifugal blower
2. Bypass valve
3. Inlet valve
4. Venturimeter
5. U-tube manometer
6. Developing section
7. Ribbed section
8. Exit section
9. Dc power source
10. Data logger
11. Laptop
12. Dpt
13. Infrared camera
14. Inlet thermocouple
15. Exit thermocouple

Figure 1: Illustration of experimental setup.

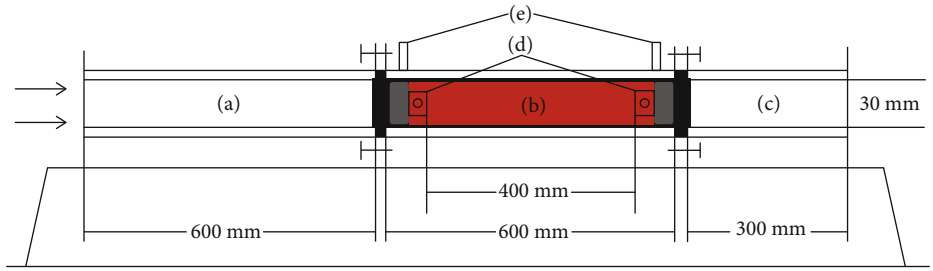

Figure 2: Schematic of (a) developing section, (b) ribbed section, and (c) exit section.

number, heat transfer increased; however, thermal performance decreased. They also concluded that the arrangement of turbulators inside enclosed spaces is an important parameter which defines the increment in heat transfer. With better arrangement of turbulators, higher heat transfer can be generated at relatively lesser flow rates. Delbari et al. [20] studied different blade profiles and established that the turbine blade aspect ratio is one of the important operational parameter, and the performance and fuel consumption depend largely on the geometry of the blade profile.

Pordanjani et al. [21] brought out that many engineering applications employ the principles of convection inside cavities. They also submitted that determination of losses and minimization of the same is considered paramount as industrial applications demand high efficiency devices. Authors Tang et al. [22] established in their work that fouling of compressor blades of a gas turbine is unavoidable, and the same has a negative effect on the overall performance and safety. Since the compressed air is used for cooling the turbine blades, it is prudent to select rib turbulators which can generate high heat transfer for low pressure drop and optimal coolant air consumption so that the inescapable reduction in overall engine performance due to fouling can be marginally compensated. Jiang et al. [23] in their research work highlighted the importance of blade cooling and selection of right alloy to prevent creep failure of rotor blades. They brought out that, in view of the rapid progression in aviation industry, necessity to operate the gas turbines at elevated temperatures for achieving higher thrust to weight ratio and performance has become inevitable. Therefore, it is of utmost importance to prevent creep failure by right selection of blade material and cooling methodology. Yousefzadeh et al. [24] researched the heat transfer inside a cavity with dissimilar areas of heat transfer. The authors concluded that by increasing fluid velocity, momentum loss increases, and in turn, pressure drop also increases due to increased collision with the surface. The authors also established that the effects of back flow reduce by increasing velocity and by decreasing the velocity, boundary layer thickness increases. Deng et al. [25] by employing 90° ribs examined the influence of three different e/D_h ratios on thermohydraulic performance inside a rotating square channel. The authors confirmed optimum performance at e/D_h ratio 0.1 for Re up to 40000. Krishnaswamy and Sivan [26] evaluated V- and W-ribs in a channel (AR = 1 : 4) and concluded that 45° V- and W-ribs with e/D_h values of 0.0729 and 0.0833 produced high thermal performances. Besides, the authors also reported that nonuniformity in heat transfer was greatest for W-ribs. Wang et al. [27] numerically investigated the cooling effectiveness of 60° inclined and V-shaped ribs in a two pass channel. They concluded by saying that under rotating condition, heat transfer increment was observed to be maximum in the trailing wall and bend regions due to rotation induced forces. Also, they established that heat transfer augmentation for V-shaped ribs was superior to angled ribs.

1.1. Novelty. Due to the airfoil shape of turbine blade, difference in height between the leading and trailing walls from the

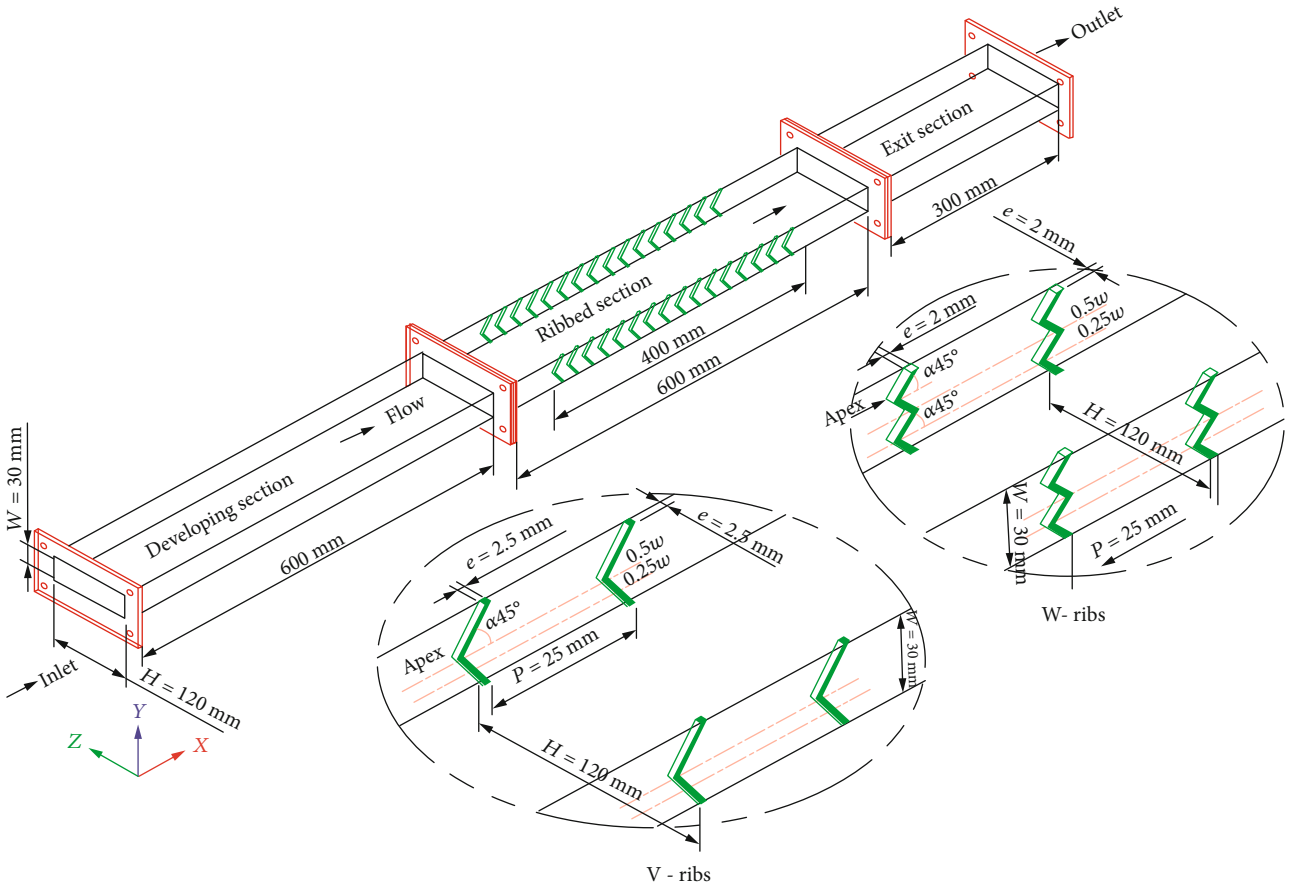

Figure 3: 3D model of test section with V- and W-shaped ribs.

Table 2: Instrument details.

Measuring device	Model and make	Accuracy	Range
Multimeter	M 3900, M/s Mastech	± 0.5%	200 mV to 1000 V
Pressure transmitter	CP 100, M/s KIMO	± 1.5%	0 to 100 Pa
Thermal camera	Ti 9, M/s Fluke	± 5°C	-20°C to 250°C
Thermocouple	*K*-type	± 0.25%	0 to 600°C
Anemometer	Testo 425	± 0.03 m/s	0 to 20 m/s

midchord increases towards the leading edge and decreases towards the trailing edge. As a result, ribbed cooling passages closer to leading edge are very narrow with aspect ratios up to 1 : 6 [26]. From the literature survey, it has been established that turbine blade aspect ratio is one of the most important operational parameter, and therefore, deployment of rib turbulators with optimal geometry is vital for optimizing the performance. Further, it is also evident that a large number of studies on blade cooling carried out till date are restricted to square and narrow ribbed cooling passages with aspect ratios up to 1 : 2, and therefore, a need is felt to assess the friction and heat transfer in narrow cooling passages adjoining the leading edge with aspect ratios lesser than 1 : 2.

Another important aspect is to effectively manage the thermal parameters near the leading edge by employing ribs that can deliver high performance. Due to high operating temperatures, thermal stresses in the areas adjoining the leading edge are exceedingly high, and hence, it is paramount to achieve maximum heat transfer with minimal friction losses and coolant consumption. As the coolant is further utilized for impingement and film cooling after exiting the ribbed passages, any effort to increase heat transfer by increasing the rib height or by reducing the rib pitch will only increase the friction losses which in turn will bring down the overall cooling effectiveness. Further, studies have concluded that the thermohydraulic performances of W- and V-shaped ribs are better than other rib profiles such as orthogonal and angled ribs because of the superiority of secondary flows produced by these ribs.

With the above background, present experimental work has been performed with an objective to maximize heat transfer and minimize pressure drop inside a ribbed passage

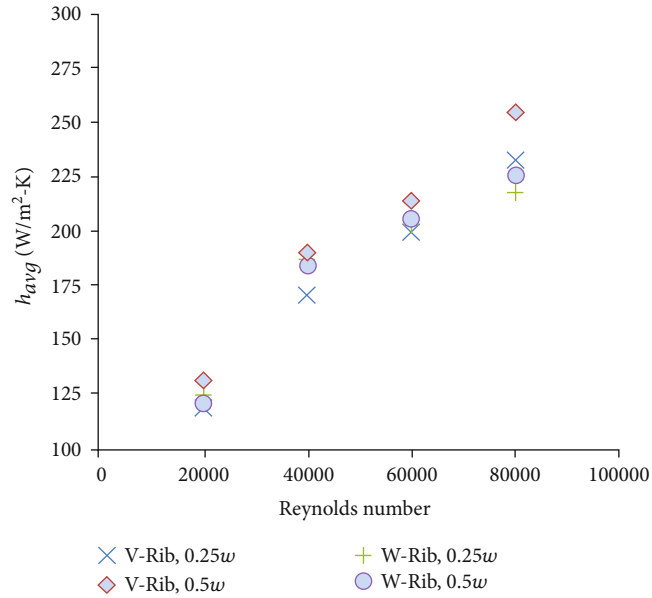

Figure 4: Variation in span averaged heat transfer coefficient (h_{avg}) with Re.

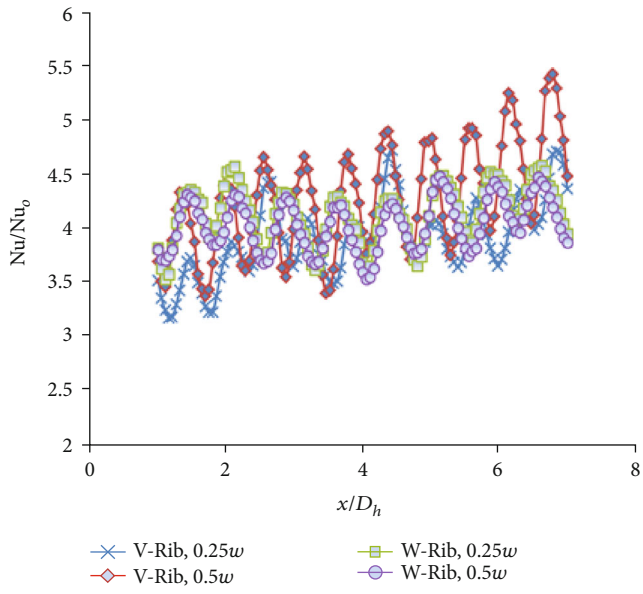

Figure 5: Streamwise variation of Nu/Nu$_o$ for Re 20000.

(AR = 1 : 4) located close to the leading edge for Re range 20000-80000. In order to achieve the objective, upstream pointing W- and V-shaped ribs are selected, and the critical geometric factors such as pitch, angle-of-attack, and rib height have been optimized. To the authors understanding and appreciation, geometry of ribs studied in the present work and same highlighted at Table 1 has been tested for the first time in a ribbed cooling passage with aspect ratio 1 : 4, and the optimized geometric parameters have provided encouraging results. Maximum and minimum thermohydraulic performances attained are 3.7 and 1.7 for Re 20000 and 80000, respectively. Considering the superior thermal performance, it can be concluded that the ribs and geometric parameters selected are ideal for effective thermal management in cooling passages near the leading edge.

2. Materials and Methods

A fabricated setup installed in the lab is illustrated in Figure 1. The atmospheric air is supplied to the system by the centrifugal blower with a maximum capacity of 1500 CFM. The discharge of the blower is passed through a calibrated venturimeter and controlled using a ball valve. Excess air is released to atmosphere through bleed valve. The flow rate is determined by the pressure head difference in the water manometer connected with the venturimeter. The venturimeter outlet is connected to test section through a 1 m pipe which houses two calibrated thermocouples (K-type) to measure inlet bulk air temperature.

Schematic of the three sections is represented in Figure 2. Test section is manufactured using a 12 mm thick acrylic sheet which is also commercially available under the brand names Plexiglas, Lucite, Perspex, and Crystallite. In the present case, acrylic material is preferred as they can withstand operating temperatures up to 120°C, possesses adequate strength and very low thermal conductivity. The test section height is 120mm, width is 30 mm, and full length is 1500 mm. The test section consists of three sections namely developing, ribbed, and exit sections. Developing section is 12.5 D_h in length to ensure the flow is developed completely prior to ribbed section, which is connected downstream. The ribbed section is also 12.5 D_h consisting of ribs on two walls. For measuring the pressure drop across ribbed section, either end of the ribbed section is provided with a pressure tap. A differential pressure transmitter (DPT) is connected to the pressure taps by using a flexible transparent hose for measuring the pressure drop. To avoid change in parameters in view of sudden expansion of air to the atmosphere, exit section of

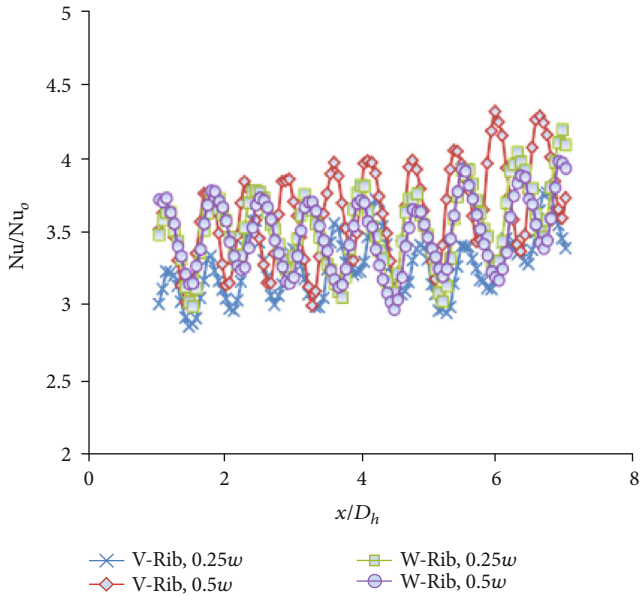

Figure 6: Streamwise variation of Nu/Nu$_o$ for Re 40000.

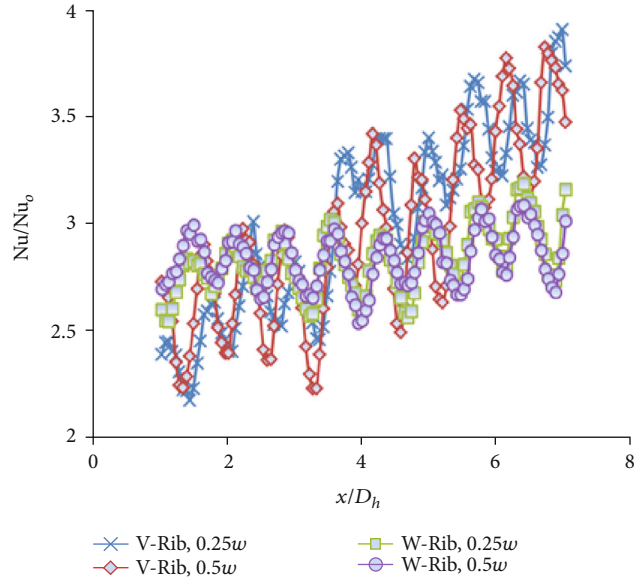

Figure 7: Streamwise variation of Nu/Nu$_o$ for Re 60000.

6.25 D_h is connected to downstream end of ribbed section. Sudden variation in velocity will influence the friction and heat transfer behaviours in ribbed section; therefore, exit section is considered important. The exit section houses two calibrated thermocouples (K-type) for measurement of exit bulk air temperature.

The two opposite ribbed walls measuring 460 mm in length and 40 mm in width are prepared using 0.2 mm thickness stainless steel sheet. Two copper blocks each of size 25 mm × 30 mm × 3 mm consisting of a brass stud at the center are soldered to either end of the sheet. After reinforcement, the effective ribbed surface area is 400 mm × 30 mm. The power is supplied to the stainless steel foil through the copper blocks. The resistance of each foil is as low as 0.0355 Ω. As

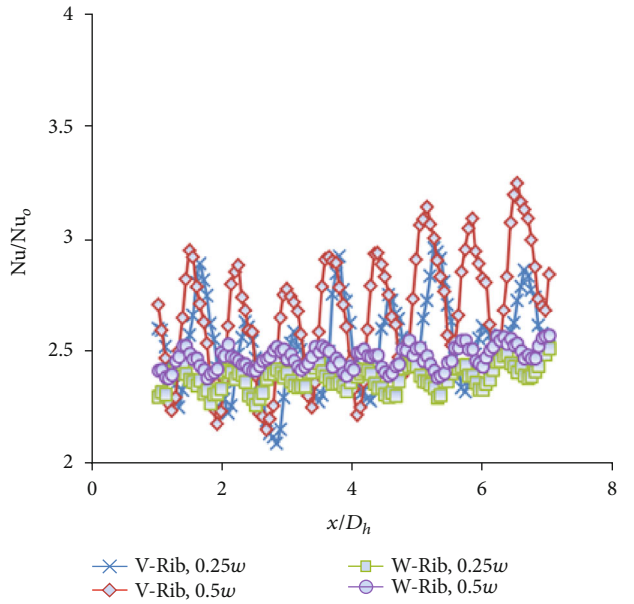

Figure 8: Streamwise variation of Nu/Nu$_o$ for Re 80000.

the thickness of the foil is very less, temperature variation between inner and outer surfaces is insignificant, and therefore, the effect due to lateral conduction has not been considered. A DC source with a maximum capacity of 1200 W (150 A and 8 V) is used to provide the required power.

The ribs under study are square in cross section and made from 2.5 mm and 2 mm balsa wood, respectively. Balsa material has been chosen as it possesses very low density, high strength to weight ratio, and widely used in studies related to aero-modeling and internal cooling of turbine blades using ribs [3]. The V-shaped ribs consist two arms which are joined along the centerline, and the W-shaped ribs consist of four arms made into two V-shapes and joined together along the centerline. Anabond silicone sealant is used to position the ribs on the foil inner surface. Subsequently, both the ribbed foils are secured to the acrylic sheet. After securing, high temperature heat resistant silicone tape is used additionally to bond the foils with the acrylic sheet. While bonding, due care is exercised to avoid air gap between the surfaces. The outer surface of the foils is painted with matt black paint for high emissivity. A thermal imaging camera has been used to measure the ribbed wall temperatures. A 3D model of test section with rib shapes is shown in Figure 3 for better appreciation.

The coolant flow rate is adjusted to achieve the differential pressure head corresponding to Reynolds number under examination. After stabilization of flow inside the test section, power source is switched on and after 30 minutes; critical parameters such as ribbed wall temperatures, pressure drop across ribbed section, inlet/exit bulk air temperatures, voltage drop across the copper blocks, and coolant velocity are recorded. Subsequently, using the infrared camera, ribbed wall images are captured and then processed to determine the wall temperatures locally. Friction factor and Nusselt number have been calculated by using the equations referred in literature.

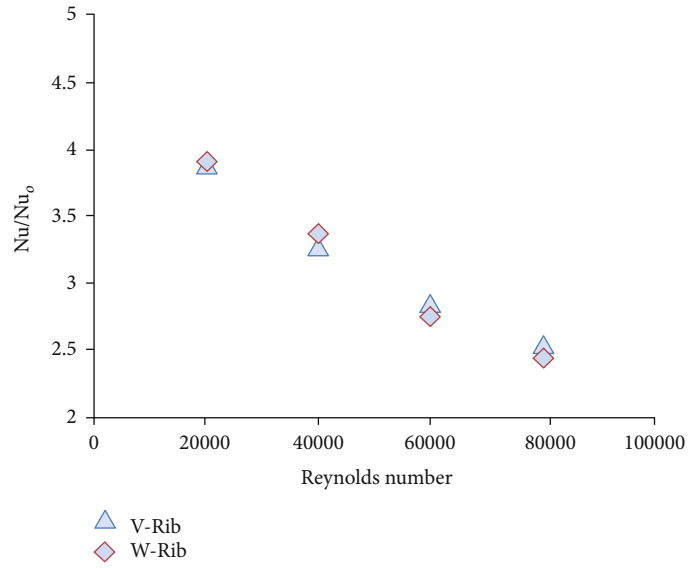

Figure 9: Variation of area averaged Nusselt number ratio with Re.

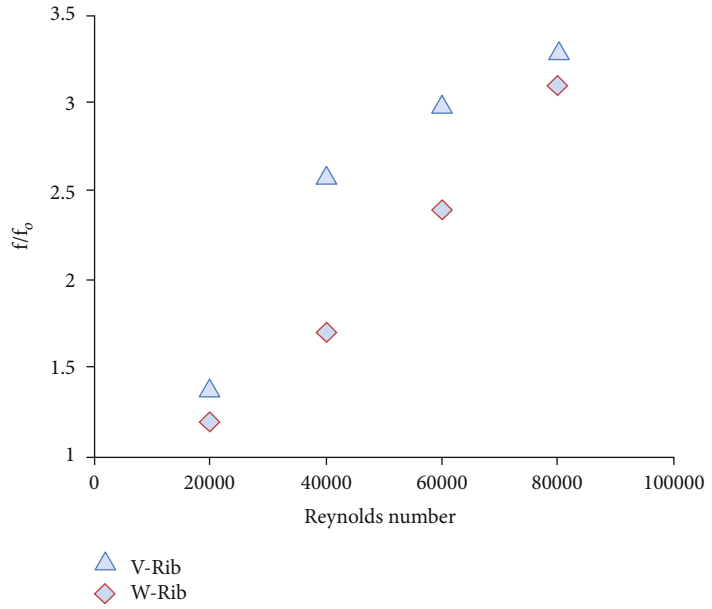

Figure 10: Normalized friction factor ratio.

The Re is determined using Eq. (1) referred in Krishnaswamy and Sivan [26].

$$\mathrm{Re} = \frac{\rho v D_h}{\mu}. \quad (1)$$

Heat input is given by Eq. (2) referred in Abraham and Vedula [3] and Deng et al. [25].

$$Q_{\text{input}} = VI. \quad (2)$$

Heat loss due to radiation and natural convection adds up to the total heat loss and the same expressed at Eq. (3) and referred in Krishnaswamy and Sivan [26]. Maximum heat loss has been found to be 10.5% of power input at Re 20000.

$$Q_{\text{loss}} = Q_{\text{rad}} + Q_{\text{conv}}. \quad (3)$$

Equation (4) referred by Abraham and Vedula [3] and Deng et al. [25] gives the net heat input.

$$Q_{\text{net}} = Q_{\text{input}} - Q_{\text{loss}}. \quad (4)$$

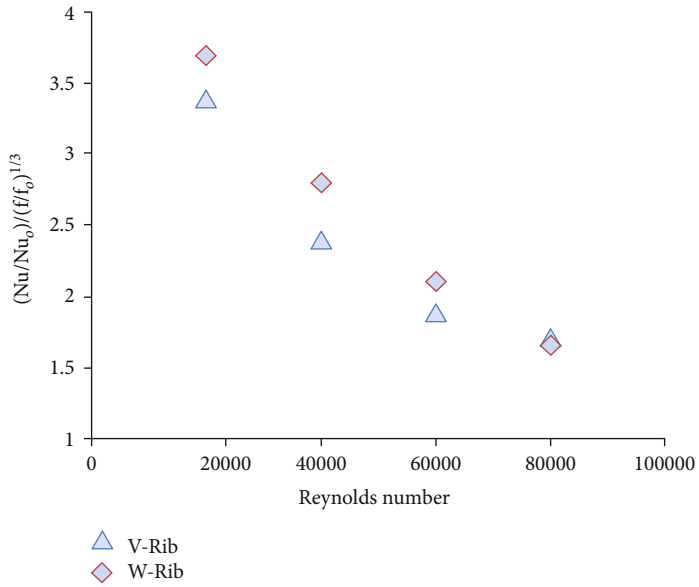

Figure 11: Thermohydraulic performance.

Table 3: Nu/Nu$_o$ comparison.

	Ribs	e/D_h	P/e	α (°)	Re	Nu/Nu$_o$
Present study	V-ribs	0.052	10	45°	20000/40000/60000	3.9/3.3/2.8
Present study	W-ribs	0.0416	12.5	45°		3.9/3.4/2.7
Abraham and Vedula [3]	V-ribs	0.08	10	45°	20000/35000	2.4/2.1
Abraham and Vedula [3]	W-ribs	0.08	10	45°		2.45/2.3
Prashant et al. [4]	V-ribs	0.125	16	45°	20000/40000/60000	3.0/2.75/2.5
Prashant et al. [4]	W-ribs	0.125	16	45°		2.5/2.4/2.1
Ravi et al. [10]	Angled ribs	0.125	16	45°	20000/40000/60000	2.25/2.2/2.15
Ravi et al. [10]	M-ribs	0.125	16	45°		1.8/1.75/1.7
Deng et al. [25]	Orthogonal ribs	0.1	—	90°	20000	3

After calculating, net heat input the energy balance is obtained from Eq. (5) used by Abraham and Vedula [3] and Deng et al. [25].

$$Q_{\text{net}} = \dot{m} c_p (T_{\text{bin}} - T_{\text{bout}}). \quad (5)$$

Inlet and exit bulk air temperatures are linearly interpolated for determining the localized bulk temperature of air. The localized bulk temperature in spanwise direction is assumed to be constant. Equation (6) referred in Deng et al. [25] is used to estimate the local heat transfer coefficient.

$$h = \frac{Q_{\text{net}}}{A(T_{\text{wall}} - T_{\text{bulk}})}. \quad (6)$$

Expression used by Omeroglu [19] and Deng et al. [25] to evaluate area averaged Nusselt number is shown in

$$\text{Nu} = \frac{\bar{h} D_h}{k}. \quad (7)$$

Equation (8) represents the Dittus-Boelter Correlation for a smooth circular pipe referred in Deng et al. [25].

$$\text{Nu}_o = 0.023\ \text{Re}^{0.8}\ \text{Pr}^{0.4}. \quad (8)$$

Nusselt number ratio used by Omeroglu [19] and Deng et al. [25] for evaluating the augmentation is represented in

$$\frac{\text{Nu}}{\text{Nu}_o}. \quad (9)$$

Ribbed wall friction factor is determined by using Eq. (10) referred in Deng et al. [25].

$$f = \frac{\Delta P D_h}{2\rho L v^2}. \quad (10)$$

Blasius equation for Turbulent Friction factor in smooth circular pipe is denoted by Eq. (11) and the same referred in

Omeroglu [19] and Deng et al. [25].

$$f_o = 0.079\ \mathrm{Re}^{-1/4}. \quad (11)$$

For constant pumping power, thermohydraulic performance is determined from Eq. (12) used by Omeroglu [19] and Deng et al. [25].

$$\mathrm{THP}\,(\eta) = \frac{(\mathrm{Nu}/\mathrm{Nu}_o)}{(f/f_o)^{1/3}}. \quad (12)$$

2.1. Validation. In the current work, uncertainties in heat transfer and friction measurements are mainly because of errors noticed in measurement of coolant flow rate and ribbed wall temperatures. Hot wire anemometer and calibrated thermocouple (K-type) have been used to validate the coolant flow rate and ribbed wall temperatures measured by the venturimeter and thermal imaging camera, respectively. The coolant velocity is estimated from the static differential head across the U-tube water manometer connected to the venturimeter. The velocity of coolant thus measured is corroborated with the velocity measured by the anemometer. For the experimented range of Re, error observed in coolant velocity ranged from 0.55 m/s to 1.25 m/s. To evaluate error in wall temperature measurement, calibrated thermocouple is fixed to a stainless steel metal sheet (0.2 mm, grade 304) coated with matt finish black paint used for painting the ribbed walls also. Thereafter, by using the DC power source, stainless steel sheet is energised gradually in steps up to 80°C. The steady state temperatures are then recorded simultaneously by the thermocouple and thermal camera. Between the camera and thermocouple measurements, a maximum error of 4°C at 80°C is observed. Thermocouples used for measurement are calibrated by using thermo water bath. The errors are found to be within ±0.05°C. The accurancy and range of measuring instruments utilized in this work are highlighted in Table 2. Using the methodology proposed by Moffat [28], maximum uncertainty in estimation of friction and Nusselt number are 8.5% and 11.5% at Reynolds number 20000.

3. Results and Discussion

The present study is aimed at evaluating thermohydraulic performance of continuous W- and V-ribs. Nusselt number ratios ($\mathrm{Nu}/\mathrm{Nu}_o$) for both rib shapes have been determined along span lengths $0.25w$ and $0.5w$. Also, friction factor across the ribbed walls has been determined to evaluate the thermohydraulic performance.

3.1. Span Averaged Heat Transfer Coefficient. Figure 4 depicts variation in span averaged heat transfer coefficients. The values improved as the Reynolds number increased and are highest along the centerline ($0.5w$) for V-shaped ribs because of dominant nature of rib generated flow separation and reattachment. For V-shaped ribs, averaged heat transfer coefficient along $0.5w$ at Re 80000 is found to be 1.94 times higher than the value measured at Re 20000. For W-shaped ribs, magnitude of averaged heat transfer coefficient along

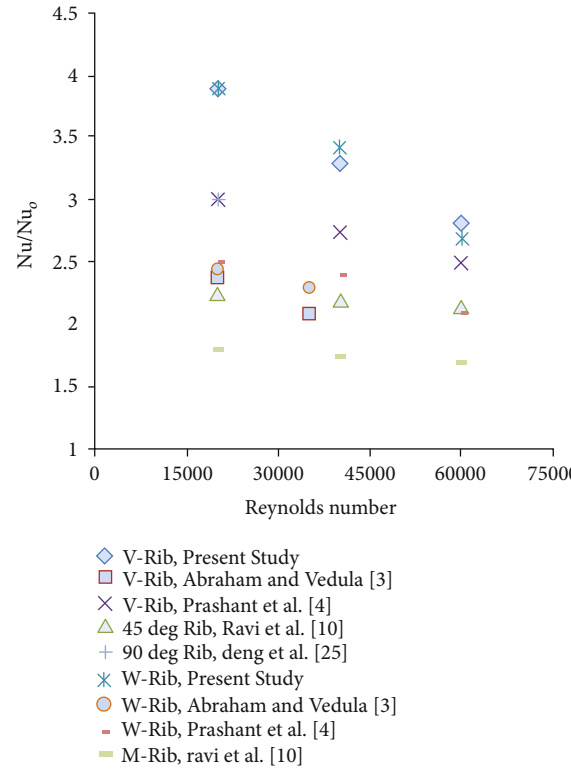

Figure 12: Comparison of $\mathrm{Nu}/\mathrm{Nu}_o$ with published data.

$0.25w$ is noticed to be highest for Re 20000 and 40000 and along $0.5w$ for Re 60000 and 80000. The value at Re 80000 is 1.8 times higher than that measured at Re 20000. Comparison of increment in values between two successive Re shows that increment is highest at 45% between the Re 20000 and 40000 for V-shaped ribs and 50% for W-shaped ribs. For Re range 40000-80000, extent of augmentation in heat transfer reduced and is noticed to be in the range of 15-18% for V-shaped ribs and 8-10% for W-shaped ribs. Reduction in increment beyond Re 40000 is due to decline in magnitude of secondary flow in the direction of stream due to coolant diversion along rib arms. The primary reason for coolant diversion is the decrease in velocity boundary layer thickness at higher Re. In addition, it is also speculated that, for the selected blockage ratio and pitch, impact induced by the ribs on flow is highest at Re 40000.

3.2. Streamwise and Spanwise Variations in Nusselt Number Ratio. In the direction of stream, heat transfer is predominantly influenced by the secondary flow generated as a result of flow separation at the rib. Along rib arms, magnitude of heat transfer depends upon the strength of counter rotating vortices generated as a result of coolant flow along the arms. In general, intensity of secondary flows is primarily influenced by the factors such as rib pitch, profile, angle-of-attack, and rib height. Nusselt numbers along the stream are highest at the reattachment zone due to very low wall temperatures produced by the high impingement velocity of the coolant. At the separation zone, Nusselt numbers are found to be relatively lower than reattachment zone. This is because,

Table 4: THP comparison.

	Ribs	e/D_h	P/e	α (°)	Re	THP
Present study	V-ribs	0.052	10	45°	20000/40000/60000	3.4/2.4/1.9
Present study	W-ribs	0.0416	12.5	45°		3.7/2.8/2.1
Abraham and Vedula [3]	V-ribs	0.08	10	45°	20000/35000	1.45/1.3
Abraham and Vedula [3]	W-ribs	0.08	10	45°		1.3/1.2
Prashant et al. [4]	V-ribs	0.125	16	45°	20000/40000/60000	1.6/1.45/1.25
Prashant et al. [4]	W-ribs	0.125	16	45°		1.45/1.2/1.05
Ravi et al. [10]	Angled ribs	0.125	16	45°	20000/40000/60000	1.15/1.1/1.05
Ravi et al. [10]	M-ribs	0.125	16	45°		0.95/0.85/0.8
Deng et al. [25]	Orthogonal ribs	0.1	—	90°	20000	1.8

magnitude of secondary flow generated in the stream direction is relatively higher than that of counter rotating vortices induced by the rib arms. After the reattachment zone, capability of the coolant to withdraw heat gradually reduces due to the development of boundary layer. This phenomenon in turn leads to a decline in extent of heat transfer in the direction of stream. Due to above phenomenon, the magnitude of Nusselt number between the two successive ribs varies along the stream in a sinusoidal manner, with maximum heat transfer at the reattachment zone and minimum heat transfer at the separation zone.

Figures 5–8 show the streamwise variations in local Nusselt number ratio along span lengths $0.25w$ and $0.5w$ for both the ribs. The variations for V-shaped ribs are 31% and 26% at Re 20000 and 80000, respectively. For W-shaped ribs, variations are 17.5% and 7% at Re 20000 and 80000, respectively. Increased height of V-shaped ribs influenced the boundary layer separation and reattachment more thereby leading to large variation in Nusselt number ratio. Further, streamwise variations are found to be greatest at lesser Re for both ribs due to dissimilarities in magnitude of heat transfer observed between the separation and reattachment zones. At higher Re , the variation reduced due to effect of stronger secondary flows along the span induced by the diverted coolant. Nusselt number ratio slowly increased in the streamwise direction because of increased turbulent mixing. The increasing trend is prominent for V-shaped rib view increased height of the rib. Also, an abrupt increase in Nusselt number ratio closer to exit of ribbed section is observed due to turbulence generated by the coolant while leaving the section.

The spanwise variation in local Nusselt number ratio for both rib shapes has also been analyzed. For experimented Re range, maximum spanwise variation for V-shaped ribs is 12%, and W-shaped ribs is 3.5%. Low variation for W-shaped ribs is because of the uniformity generated in view of turbulent mixing of secondary flow induced by two apexes. Also, due to the presence of additional rib arms, magnitude of counter rotating vortices generated by W-shaped ribs along the rib arms is superior in comparison to the vortices generated by V-shaped ribs. In addition, due to shorter length of rib arms, coolant is less warm, and hence, its capacity to extract heat is more for W-shaped ribs. In view of the above reasons, spanwise variations are lowest for W-shaped ribs.

3.3. Area Averaged Normalized Nusselt Number. Figure 9 depicts variation of area averaged Nusselt number ratio. Maximum difference between W- and V-shaped ribs is 3.5% at Reynolds number 80000, which is within the uncertainty limits. Low variation is because of the fact that secondary flow strength along stream for V-shaped ribs having 25% greater rib height is higher than the magnitude of secondary flow along the stream induced by W-shaped ribs. The higher strength of secondary flow along the stream for V-shaped ribs compensated for the increased strength of counter rotating vortices generated by W-shaped ribs, which in turn resulted in low variation. Nu/Nu_o for the rib profiles decreased as the Re increased. For V-shaped ribs, values are observed to be 3.9 and 2.5 corresponding to Re 20000 and 80000, respectively. At Re 40000, the Nu/Nu_o is estimated as 3.3, and at Re 60000, the value is 2.8. For W-shaped ribs, Nu/Nu_o values for Re 20000 and 80000 are estimated to be 3.9 and 2.4, respectively. For the Re 40000 and 60000, the respective values are 3.4 and 2.7. In general, Nu/Nu_o for both the rib profiles are observed to be high which is attributed to greater strength of secondary flows produced by the ribs deployed inside the narrow cooling passage. Also, to enhance the power and performance of the engine, high and uniform heat transfer augmentations are desired. While both the configurations are recommended for deployment in regions exposed to extreme temperatures, W-shaped ribs are preferred over V-shaped ribs in view of low heat transfer variations in the direction of stream and span.

3.4. Normalized Friction Factor. In a ribbed cooling passage, magnitude of friction loss is primarily dependent on the pressure drop generated by ribs. Figure 10 depicts variations in friction factor ratio. For Re range, investigated friction factor ratios for V-shaped ribs ranged from 1.4 to 3.3, and for W-shaped ribs, it ranged from 1.2 to 3.1. Friction factor ratio increased with increase in Re. Friction factor ratios are highest for V-shaped ribs due to a 25% greater height-to-channel hydraulic diameter ratio. Highest and lowest differences between friction factor ratios of the ribs are 53% and 6.5% corresponding to Re 40000 and 80000. Normalized friction factor for both ribs has been independently examined, and a maximum increase of 85% for V-shaped ribs and 42% for W-shaped ribs has been observed between Re 20000 and 40000. For both rib shapes, increment in friction factor ratio

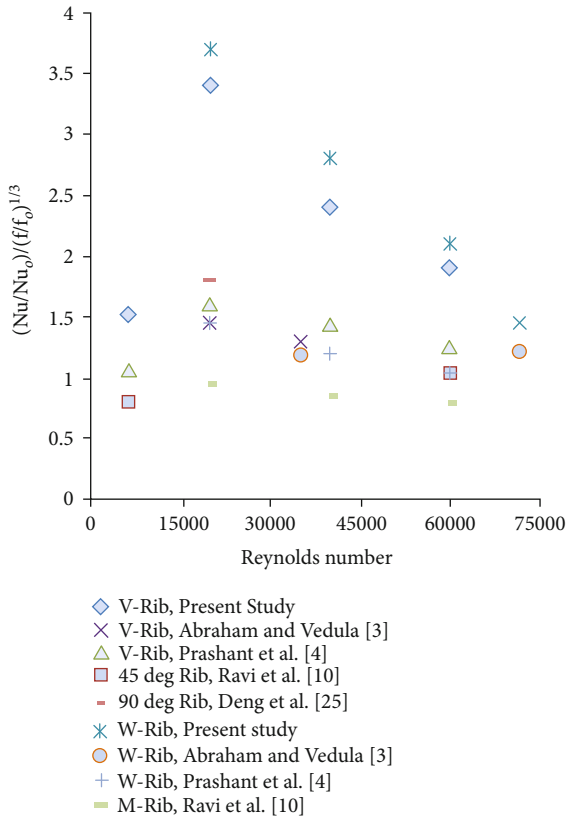

Figure 13: Comparison of THP with published data.

between successive Re beyond Re 40000 reduced due to surge in flow of coolant towards side walls owing to diversion, which consecutively decreased the overall pressure drop. In comparison to V-shaped ribs, reduction in increment is found to be lower for W-shaped ribs because the diverted coolant resulted to a surge in concentration of coolant along the centerline due to the converging rib arms, which generated a reasonable pressure drop. Despite the above phenomenon, overall pressure drop due to V-shaped ribs continued to remain higher than W-shaped ribs due to greater rib height.

3.5. Thermohydraulic Performance. Figure 11 illustrates variation in thermohydraulic performances of W- and V-shaped ribs. THP values for W-shaped ribs are higher than V-shaped ribs for Re range 20000-60000. Variation in THP is 8.8%, 16.6%, and 10.5% for Re 20000, 40000, and 60000, respectively. As it can be seen, despite low variation (3.5%) in heat transfer enhancements estimated for both rib shapes, variation in THP estimated at Re 40000 is highest owing to high pressure drop generated by the V-shaped ribs. Beyond Re 40000, variation starts reducing due to the overall decline in pressure drop owing to coolant diversion. At Re 80000, THP of V-shaped ribs is 2.5% greater than W-shaped ribs.

3.6. Comparative Study. Normalized Nusselt numbers of the rib shapes under study are compared with the published results in Table 3 and the same represented in Figure 12. Nu/Nu$_o$ values estimated for V-shaped ribs ($e/D_h = 0.052$) at Re 20000 and 35000 are 60-66% higher than V-ribs ($e/D_h = 0.08$) placed inside a converging duct studied by Abraham and Vedula [3]. In comparison to the results presented for V-ribs ($e/D_h = 0.125$) in an aspect ratio 1 : 1 channel by Prashant et al. [4], Nu/Nu$_o$ values for V-shaped ribs having blockage ratio 0.052 are 12-30% higher for the range of Re 20000 to 60000. Compared to Nu/Nu$_o$ values estimated by Ravi et al. [10] for 45° angled ribs ($e/D_h = 0.125$) in a channel having aspect ratio 1 : 1, V-shaped ribs used in this work generated 30-73% higher enhancement for Re range 20000 to 60000. The enhancement reported by Deng et al. [25] for orthogonal ribs ($e/D_h = 0.1$) in an aspect ratio 1 : 1 channel is found to be 30% less than the enhancement estimated at Re 20000 for V-shaped ribs. Similar to V-shaped ribs, Nu/Nu$_o$ values of W-shaped ribs are also noticed to be higher than that presented in literature. As compared with the enhancement predicted by Abraham and Vedula [3] for Re 20000 and 35000 for W-ribs ($e/D_h = 0.08$) inside a converging channel, enhancement due to W-shaped ribs ($e/D_h = 0.0416$) in the current work is found to be 48-60% higher. Further, when compared with the predictions of Prashant et al. [4] for continuous W-ribs for the Re 20000-60000, Nu/Nu$_o$ values estimated for W-shaped ribs in this work are 30-56% higher. Besides, the enhancements due to W-shaped ribs are found to be higher by 60-100% than that predicted by Ravi et al. [10] for continuous M-ribs ($e/D_h = 0.125$). As compared with the enhancement predicted by Deng et al. [25] for 90° ribs ($e/D_h = 0.1$) in a aspect ratio 1 : 1 channel, enhancement due to W-shaped ribs at Re 20000 is noticed to be 30% higher. Thermohydraulic performance values of V-shaped ribs and W-shaped ribs have been compared with different rib configurations, and the same are shown in Table 4 and Figure 13. For the experimented Re, the THP values of V- and W-shaped ribs used in this work are 50% to 200% greater than that presented for different rib configurations such as V-ribs, W-ribs, M-ribs, and angled ribs inside cooling channels. In addition, THP value of V- and W-shaped ribs observed at Re 20000 is 90% higher than that predicted at Re 20000 by Deng et al. [25] for 90° ribs inside a square channel with higher blockage ratio. Hence, from the comparative study, it can be concluded that the overall thermal performance due to W- and V-shaped ribs with low e/D_h ratio is superior to other configurations due to high heat transfer generated by the ribs for low friction losses. Therefore, rib configurations are recommended for deployment in regions adjacent to leading edge for enhancing the heat transfer with no major effect on friction loss.

4. Conclusions

The present experimental work has been performed with an objective to maximize heat transfer and minimize pressure drop inside a ribbed passage (AR = 1 : 4) located close to the leading edge for Re range 20000-80000 using V- and W-shaped ribs. Nusselt number ratio (Nu/Nu$_o$) and thermohydraulic performance (THP) values for the experimented Re are found to reasonably good for both the rib profiles. The following are concluded based on the analysis of results.

(1) For increase in Reynolds number, friction factor ratio increased, and Nusselt number ratio decreased

(2) In case of V-shaped ribs, extent of heat transfer at Re 20000 is 94% higher than *Re* 80000. For W-shaped ribs, the increase is 80%

(3) Maximum difference in area averaged Nusselt number ratio between both ribs is 3.5%, which is within the uncertainty limits

(4) Maximum streamwise variation in local Nusselt number ratio of V-shaped ribs is 31% at Re 20000. For W-shaped ribs, variation is 17.5% at same Re

(5) Maximum spanwise variation in local Nusselt number ratio of V-shaped ribs is 12%. For W-shaped ribs, variation estimated is 3.5

(6) Friction losses for V-shaped ribs are greater than W-shaped ribs for Re range investigated

(7) Minimum and maximum differences between the friction factor ratios of the rib shapes are 6.5% and 53% corresponding to Re 80000 and 40000

(8) For both the rib shapes, impact of ribs on friction and heat transfer is noticed to be greatest at Re 40000

(9) Highest and lowest THP values achieved with V-ribs are 3.4 and 1.7 at Re 20000 and 80000. For W-ribs, values are 3.7 and 1.65

4.1. Recommendation. In a turbine blade, large variations in heat transfer coefficient will lead to formation of hotspots and failure of the blade subsequently due to thermal stresses. Further, increase in weight of the blade due to ribs will reduce the power-to-weight ratio. While both the rib profiles generated reasonably good Nu/Nu_o and THP values, based on above conclusions, W-shaped rib which generated higher THP, lower heat transfer coefficient variations, and 25% lesser height is recommended for effective thermal management and improvised engine performance.

Nomenclature

α: Angle of attack, degree (°)
P: Rib pitch, mm
e: Height of the rib, mm
D_h: Hydraulic diameter of test section, m
W: Width of the test section, mm
H: Height of the test section, mm
v: Velocity of air, m/s
w: Width of the ribbed wall, mm
$\dot{m}$: Mass flow rate, kg/s
h: Local heat transfer coefficient, W/m^2-K
h_{avg}: Span averaged heat transfer coefficient, W/m^2-K
$\bar{h}$: Area averaged heat transfer coefficient for ribbed wall, W/m^2-K
Nu: Area averaged Nusselt number
Nu_o: Nusselt number for smooth circular pipes (Dittus-Boelter correlation)
Pr: Prandtl number
v: Streamwise air velocity, m/s
ρ: Density of air, kg/m^3
μ: Dynamic viscosity of air, N s/m^2
k: Thermal conductivity of air, W/m-K
Q_{input}: Heat input, W
Q_{loss}: Heat loss, W
Q_{net}: Net heat input, W
Q_{conv}: Heat loss due to natural convection, W
Q_{rad}: Heat loss due to radiation, W
A: Effective surface area of ribbed wall, m^2
L: Length between the pressure taps, m
T_{bulkv}: Bulk air temperature, K
T_{bin}: Bulk air inlet temperature, K
T_{bout}: Bulk air outlet temperature, K
T_{wall}: Wall temperature, K
c_p: Specific heat of air, J/kg K
I: Current, ampere (A)
V: Voltage, volt (V)
f: Friction factor
f_o: Friction factor in smooth circular pipe (Blasius friction factor)
η: Thermohydraulic performance
ΔP: Pressure drop across the ribbed section, N/m^2
A: Ampere
V: Volt
Ω: Ohms
W: Watt
Pa: Pascal.

Abbreviations

CFM: Cubic feet per minute
DC: Direct current
DPT: Differential pressure transmitter.

Data Availability

Data will be made available on request made to corresponding author.

Conflicts of Interest

The authors declare that there is no conflict of interest regarding the publication of this paper.

References

[1] M. Goodarzi, M. R. Safaei, K. Vafai et al., "Investigation of nanofluid mixed convection in a shallow cavity using a two-phase mixture model," *International Journal of Thermal Sciences*, vol. 75, pp. 204–220, 2014.

[2] M. Goodarzi, M. R. Safaei, A. Karimipour et al., "Comparison of the Finite Volume and Lattice Boltzmann Methods for Solving Natural Convection Heat Transfer Problems inside Cavities and Enclosures," *Abstract and Applied Analysis*, vol. 2014, Article ID 762184, 15 pages, 2014.

[3] S. Abraham and R. P. Vedula, "Heat transfer and pressure drop measurements in a square cross-section converging

Channel with V and W rib turbulators," *Experimental Thermal and Fluid Science*, vol. 70, pp. 208–219, 2016.

[4] P. Singh, B. V. Ravi, and S. V. Ekkad, "Experimental and numerical study of heat transfer due to developing flow in a two-pass rib roughened square duct," *International Journal of Heat and Mass Transfer*, vol. 102, pp. 1245–1256, 2016.

[5] N. G. Ghodake, C. Rao, and R. R. Arakerimath, "Flow and heat transfer analysis of various ribs for forced convection heat transfer," *Journal of Emerging Technologies and Innovative Research*, vol. 3, no. 7, pp. 42–47, 2016.

[6] W. Yang, S. Xue, Y. He, and W. Li, "Experimental study on the heat transfer characteristics of high blockage ribs channel," *Experimental Thermal and Fluid Science*, vol. 83, pp. 248–259, 2017.

[7] H. Deng, Y. Li, Z. Tao, G. Xu, and S. Tian, "Pressure drop and heat transfer performance in a rotating two-pass channel with staggered 45-deg ribs," *International Journal of Heat and Mass Transfer*, vol. 108, pp. 2273–2282, 2017.

[8] P. Singh, W. Li, S. V. Ekkad, and J. Ren, "A new cooling design for rib roughened two-pass channel having positive effects of rotation on heat transfer enhancement on both pressure and suction side internal walls of a gas turbine blade," *International Journal of Heat and Mass Transfer*, vol. 115, pp. 6–20, 2017.

[9] P. Singh, W. Li, S. V. Ekkad, and J. Ren, "Experimental and numerical investigation of heat transfer inside two-pass rib roughened duct (AR = 1:2) under rotating and stationary conditions," *International Journal of Heat and Mass Transfer*, vol. 113, pp. 384–398, 2017.

[10] B. V. Ravi, P. Singh, and S. V. Ekkad, "Numerical investigation of turbulent flow and heat transfer in two-pass ribbed channels," *International Journal of Thermal Sciences*, vol. 112, pp. 31–43, 2017.

[11] L. Wang, S. Wang, X. Zhou, F. Wen, and Z. Wang, "Numerical prediction of 45 ° angled ribs effects on U-shaped channels heat transfer and flow under multi conditions," *International Journal of Turbo & Jet-Engines*, vol. 37, no. 1, pp. 41–59, 2017.

[12] P. Singh, Y. Ji, and S. V. Ekkad, "Experimental and numerical investigation of heat and fluid flow in a square duct featuring criss-cross rib patterns," *Applied Thermal Engineering*, vol. 128, pp. 415–425, 2018.

[13] S. Ruck and F. Arbeiter, "Detached eddy simulation of turbulent flow and heat transfer in cooling channels roughened by variously shaped ribs on one wall," *International Journal of Heat and Mass Transfer*, vol. 118, pp. 388–401, 2018.

[14] T. M. Liou, S. W. Chang, and S. P. Chan, "Effect of rib orientation on thermal and fluid-flow features in a two-pass parallelogram channel with abrupt entrance," *International Journal of Heat and Mass Transfer*, vol. 116, pp. 152–165, 2018.

[15] J. Wang, J. Liu, L. Wang, B. Sundén, and S. Wang, "Numerical investigation of heat transfer and fluid flow in a rotating rectangular channel with variously-shaped discrete ribs," *Applied Thermal Engineering*, vol. 129, pp. 1369–1381, 2018.

[16] A. Aghaei, G. A. Sheikhzadeh, M. Goodarzi, H. Hasani, H. Damirchi, and M. Afrand, "Effect of horizontal and vertical elliptic baffles inside an enclosure on the mixed convection of a MWCNTs-water nanofluid and its entropy generation," *European Physical Journal Plus*, vol. 133, no. 11, article 12278, 2018.

[17] P. S. Patil, "Recent studies in internal cooling of gas turbine blade : a review," *International Journal of Applied Engineering Research*, vol. 13, no. 9, pp. 7131–7141, 2018.

[18] A. M. Aboghrara, M. A. Alghoul, B. T. H. T. Baharudin et al., "Parametric study on the thermal performance and optimal design elements of solar air heater enhanced with jet impingement on a corrugated absorber plate," *International Journal of Photoenergy*, vol. 2018, Article ID 1469385, 21 pages, 2018.

[19] G. Ömeroğlu, "CFD analysis and electrical efficiency improvement of a hybrid PV/T panel cooled by forced air circulation," *International Journal of Photoenergy*, vol. 2018, Article ID 9139683, 11 pages, 2018.

[20] S. H. Delbari, A. Nejat, M. H. Ahmadi, A. Khaleghi, and M. Goodarzi, "Numerical modeling of aeroacoustic characteristics of different savonius blade profiles," *International Journal of Numerical Methods for Heat and Fluid Flow*, vol. 30, no. 6, pp. 3349–3369, 2019.

[21] A. Hajatzadeh Pordanjani, S. Aghakhani, A. Karimipour, M. Afrand, and M. Goodarzi, "Investigation of free convection heat transfer and entropy generation of nanofluid flow inside a cavity affected by magnetic field and thermal radiation," *Journal of Thermal Analysis and Calorimetry*, vol. 137, no. 3, article 7982, pp. 997–1019, 2019.

[22] J. Tang, D. Gao, L. Wang, and J. Huo, "Experimental study on the distribution trends of fouling on a compressor blade," *International Journal of Photoenergy*, vol. 2020, Article ID 8885737, 7 pages, 2020.

[23] L. Jiang, X. Dou, and M. Wu, "Effect of stress on creep behavior of single crystal alloy IC6SX at 980°C," *International Journal of Photoenergy*, vol. 2020, Article ID 8844874, 5 pages, 2020.

[24] S. Yousefzadeh, H. Rajabi, N. Ghajari, M. M. Sarafraz, O. A. Akbari, and M. Goodarzi, "Numerical investigation of mixed convection heat transfer behavior of nanofluid in a cavity with different heat transfer areas," *Journal of Thermal Analysis and Calorimetry*, vol. 140, no. 6, article 9018, pp. 2779–2803, 2019.

[25] H. Deng, H. Li, Z. Tao, L. Qiu, and J. Zhu, "Effect of blockage ratio on heat transfer and pressure drop in rotating ribbed channels at high rotation numbers," *Journal of Thermal Science*, vol. 30, no. 3, article 1275, pp. 902–913, 2021.

[26] K. Krishnaswamy and S. Sivan, "Improvement in thermal hydraulic performance by using continuous V and W-shaped rib turbulators in gas turbine blade cooling application," *Case Studies in Thermal Engineering*, vol. 24, article 100857, 2021.

[27] X. Wang, H. Xu, J. Wang, W. Song, and L. Wang, "High pressure turbine blade internal cooling in a realistic rib roughened two-pass channel," *International Journal of Heat and Mass Transfer*, vol. 170, article 121019, 2021.

[28] R. Moffat, "Describing the uncertainties in experimental results," *Experimental Thermal and Fluid Science*, vol. 1, no. 1, pp. 3–17, 1988.